

A NUMERICAL SIMULATION OF HYDRODYNAMIC FORCES OF GROUND-EFFECT PROBLEM USING LAGRANGE'S EQUATION OF MOTION

SHIH-AN YANG* AND PAN-AN LUH

Department of Naval Architecture and Marine Engineering, National Cheng Kung University, Tainan, Taiwan, Province of China

SUMMARY

On the basis of the potential flow theory, Lagrange's equation of motion is used to study the unsteady ground-effect problem. The forces and moments acting on the moving body are solved in terms of the derivatives of added masses in which the generalized Taylor's formulae are applied. The singular integral equations used to solve the surface source intensities and their derivatives are regularized by the Gauss flux theorem and are therefore amenable to the direct use of the Gaussian quadrature formula. In illustration, the condition of a prolate spheroid moving in the fore-and-aft direction at constant speed past a flat ground with a protrusion is considered. The hydrodynamic forces and moments acting on the moving spheroid are investigated systematically by varying the size of the protrusion and the cruising height of the spheroid. © 1998 John Wiley & Sons, Ltd.

KEY WORDS: unsteady two-body interaction; potential flow theory; boundary-integral method; Lagrange's equation of motion; generalized Taylor's formula

1. INTRODUCTION

The study of hydrodynamic interactions between two bodies has received much attention for several decades, either in the unbounded fluid domain [1,2] or in the fluid field with a free surface [3]. The applications extend to a variety of topics, such as the impact of floating ice floes with the protrusion, the motion of ships in restricted waterways, the operation of vessels near a pier, submersibles moving near the seabed, and so on. As long as the corresponding bodies are not very close together, the potential flow theory will provide acceptable results. There are several methods with which to approach the associated topic. The first category, which is virtually an extension of the thin-wing theory, uses the slender-body theory combined with the technique of matched asymptotic expansions. Tuck [4,5] initiated the procedure and studied the steady motion of ships in shallow water. The lateral motion of a slender body between two parallel walls was treated by Newman [6]. It was found that the walls generally increase the magnitude of interaction forces and moments on the body. Tuck and Newman [7] considered the situation where vessels are stationary in relation to each other and the flow is steady. The dynamic effects on a moored vessel resulting from the passing of another ship were

* Correspondence to: Department of Naval Architecture and Marine Engineering, National Cheng Kung University, Tainan, Taiwan 70101, Province of China.

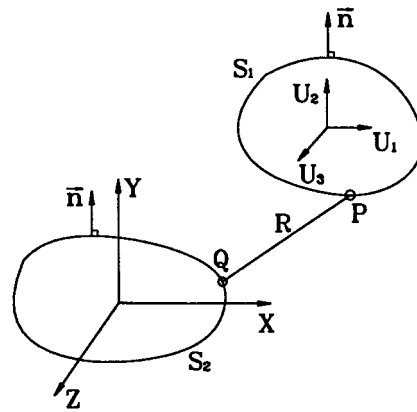


Figure 1. Interaction of two bodies.

solved by Wang [8]. The forces and moments were evaluated by application of the Lagally theorem. King [9] treated unsteady interactions between ships in very shallow water and used a Kutta condition on moving bodies. In contrast to previous authors, Yeung and Hwang [10] carried out the nearfield interactions of ships in shallow water. Therefore, a detailed knowledge of the hull geometry is required. Other versions of the theory and its applications can be found in the works of Yeung [11], Hess [12], Yeung and Tan [13], Davis and Geer [14] and Davis [15].

The second approach is the boundary-integral method combined with Lagrange's equation of motion. Chow *et al.* [16] presented the results for the velocity potentials, added masses and several of the hydrodynamic force and moment coefficients for a spheroid emerging into a fluid from an infinite, moving plane. The Kelvin–Kirchhoff form of equations of motion for a moving body in the presence of other fixed boundaries is due to Miloh and Landweber [17]. Landweber and Chwang [18] generalized Taylor's added-mass formula and [19] applied the theory, coupled with the equation of motion, to the case of a floating rectangular cylinder approaching a fixed circular cylinder. Guo and Chwang [20,21] further extended the method to study the hydrodynamic effects of two circular cylinders and two spheres. The trajectories of moving bodies were calculated to simulate the motion of floating ice floes which were conveyed by an oncoming stream around the protrusion, and to predict whether the floating body would

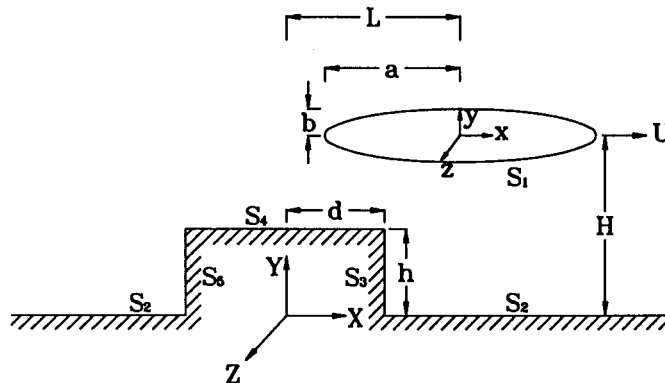


Figure 2. Interaction between a translating spheroid and a platform.

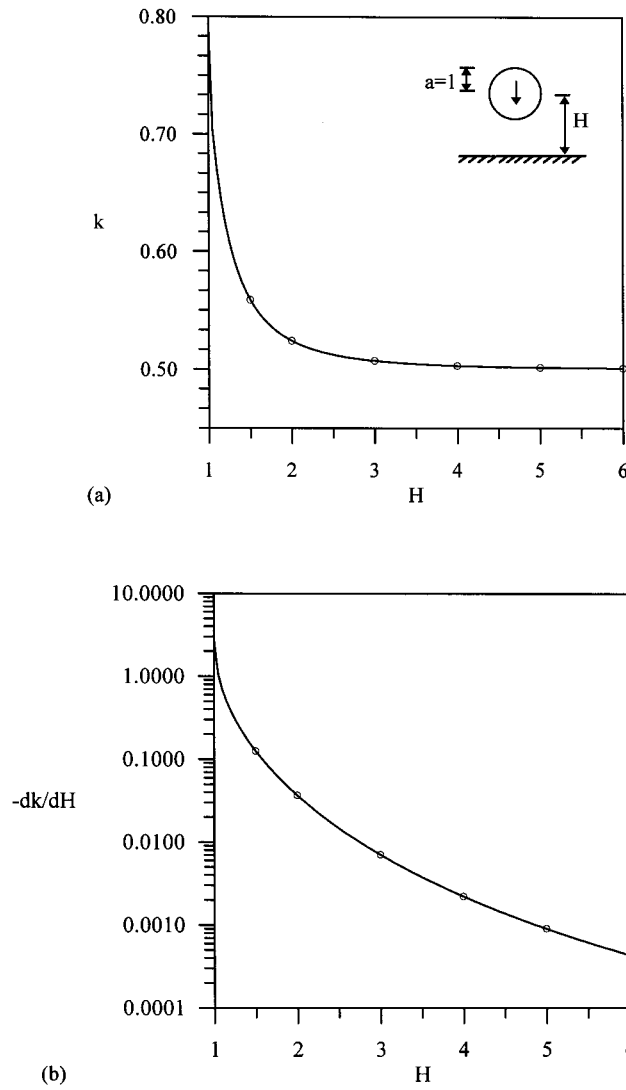


Figure 3. (a) Added-mass coefficients k and (b) their derivatives dk/dH for a sphere moving perpendicular to a plane wall. (—) Analytic solution; (○) numerical solution.

be in contact with the support structure. For a more general Lagrange's equation including a free surface, one can refer to the works by Miloh and Hauptman [22], Miloh [23] and Athanassoulis and Loukakis [24].

In the present work, Lagrange's equation of motion is adopted to deal with the ground-effect problem. In particular, a prolate spheroid moving in the fore-and-aft direction at constant speed, in the proximity of the flat ground with a protrusion is considered. The unknown source strengths are distributed on the body surfaces. Application of the boundary conditions results in a set of Fredholm integral equations of the second type. For the accuracy and convenience of the numerical implementation, the singular integrals are regularized by the Gauss flux theorem. The source strengths are solved by the iterative method after discretizing integral equations using the Gaussian quadrature formula. The forces and moments acting on the

moving spheroid are computed in terms of Lagrange's equations of motion, in which the required added masses and their derivatives are obtained using the generalized Taylor's formula. The Euler angles in the xyz -convention are introduced for the calculation of the moments. Several step sizes and cruising heights will be considered. Our principal objective is then to investigate the variations of the forces and moments acting on the moving spheroid.

2. MATHEMATICAL FORMULATION

The mathematical theory of boundary-integral method for the two-body interaction problem can be found in the works quoted in the last section. For the sake of completeness, we outline the algorithm in this section in a relatively compact pattern, but without losing the generality. Consider a body translating with three degrees of freedom, U_1 , U_2 and U_3 , without rotation in the proximity of a fixed obstacle (Figure 1). The XYZ Cartesian co-ordinate system is fixed in space. The formulation to be presented in the following will be slightly more general than required in the next section, with only U_1 remaining. The fluid is assumed to be incompressible and non-viscous. The flow is irrotational and is at rest at infinity. There exists a velocity potential ϕ that satisfies the Laplace equation, $\nabla^2\phi = 0$, and can be expressed as

$$\phi = U_i\phi_i, \quad i = 1, 2, 3, \quad (1)$$

where ϕ_i is the unit velocity potential due to the i th velocity component of the body when $U_i = 1$ and other two velocities are zero. A repeated index indicates summation in Equation (1). The kinematic boundary condition on the surface of moving body S_1 is

$$\left. \frac{\partial\phi}{\partial n} \right|_{S_1} = U_i n_i, \quad i = 1, 2, 3, \quad (2)$$

where n_i denotes the i th component of the unit vector \vec{n} in the direction of the normal drawn outward from the solid body. Also on the surface of the fixed body S_2 ,

$$\left. \frac{\partial\phi}{\partial n} \right|_{S_2} = 0. \quad (3)$$

Applying the method of surface source distribution, we have the well-known relationship at a field point Q on the surface S_i

$$\left. \frac{\partial\phi}{\partial n} \right|_{S_i} = 2\pi\sigma_Q - \iint_{S_1+S_2} \sigma_P \frac{\partial}{\partial n_Q} \left(\frac{1}{R} \right) dS, \quad i = 1, 2, \quad (4)$$

where σ_Q and σ_P denote the source strengths at the field point Q and source point P respectively, n_Q the normal at the field point, and R the distance from the source point to the field point. In order to remove the singularity as $R = 0$ in Equation (4) we apply the Gauss flux theorem, which states that the flux through a closed surface due to a unit source on the same surface is 2π :

$$- \iint \frac{\partial}{\partial n_p} \left(\frac{1}{R} \right) dS = 2\pi, \quad (5)$$

where $\partial/\partial n_p$ represents the differentiation in the normal direction at the source point P . Equation (4) can then be modified to the form

$$\left. \frac{\partial\phi}{\partial n} \right|_{S_i} = 4\pi\sigma_Q + \iint_{S_1+S_2} \left[\sigma_Q \frac{\partial}{\partial n_p} \left(\frac{1}{R} \right) - \sigma_P \frac{\partial}{\partial n_Q} \left(\frac{1}{R} \right) \right] dS, \quad i = 1, 2. \quad (6)$$

These are Fredholm integral equations of the second kind. The integrand in the right member of Equation (6) is set equal to zero when P coincides with Q . The source distributions can be solved if the velocity of the moving body is provided.

The classical Lagrange's equations for describing the motion of bodies in fluid are given by Lamb [25]

$$\frac{d}{dt} \frac{\partial T}{\partial \dot{q}_i} - \frac{\partial T}{\partial q_i} = Q_i, \tag{7}$$

where T denotes the total kinetic energy, t is the time, \dot{q}_i the generalized velocities, q_i the generalized co-ordinates and Q_i the generalized forces. The total kinetic energy in the present problem can be written as

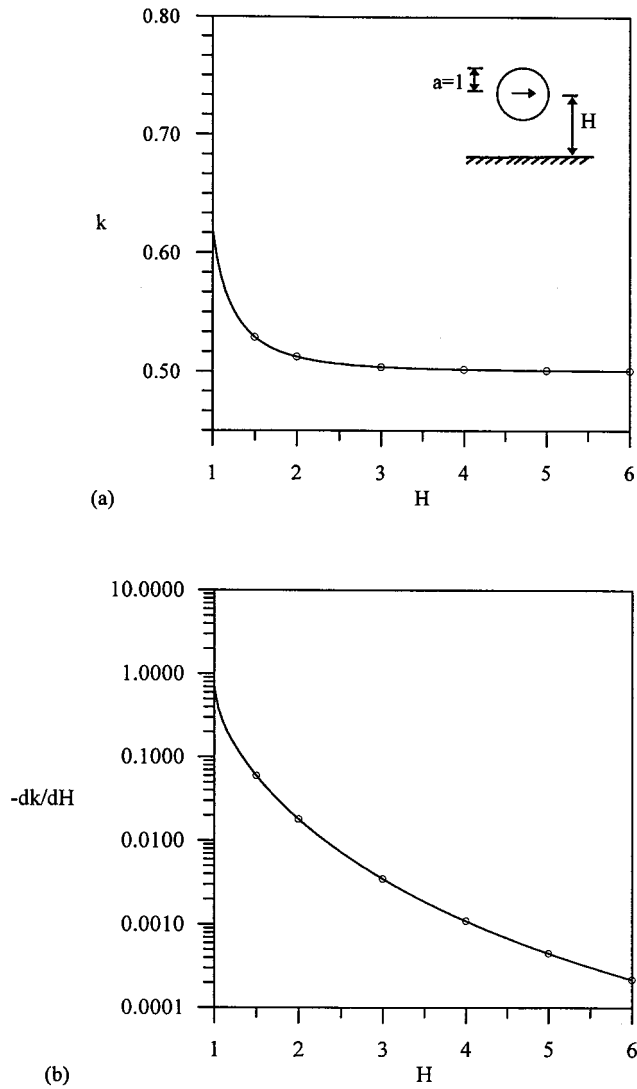


Figure 4. (a) Added-mass coefficients k and (b) their derivatives dk/dH for a sphere moving parallel to a plane wall. (—) Analytic solution; (○) numerical solution.

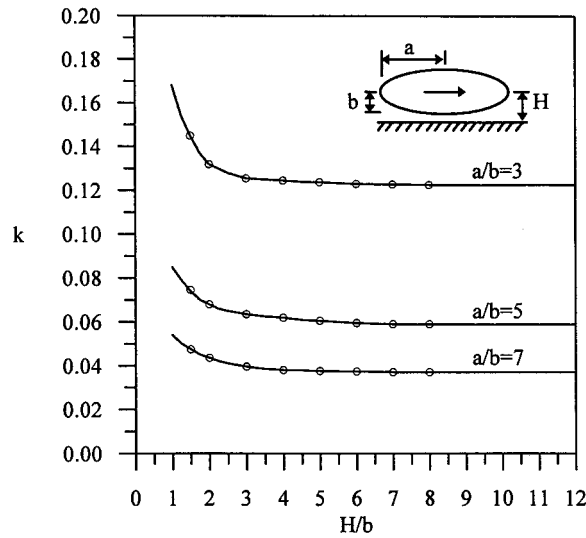


Figure 5. Added-mass coefficients for a spheroid moving parallel to a plane wall. (—) Analytic solution; (○) numerical solution.

$$2T = mU_i^2 + A_{ij}U_iU_j, \quad i, j = 1, 2, 3, \tag{8}$$

where m denotes the mass of the moving body and A_{ij} the added masses. The extended Taylor theorem expresses added masses in terms of source distributions in the following [18]:

$$A_{ij} = -m'\delta_{ij} + 4\pi\rho \iint x_j\sigma_i \, dS, \quad i, j = 1, 2, 3, \tag{9}$$

where m' is the mass of the fluid displaced by the moving body, δ_{ij} is the Kronecker delta, ρ is the fluid density, σ_i is the surface source distribution on the body due to unit motion in the i th direction, and x_j is the local co-ordinate of σ_i . We notice that (6)–(9) construct the basic equations that are used to analyze the forces and moments exerted on the moving body or the trajectories of motion. The following section provides numerical examples that may offer some useful engineering applications.

3. PROBLEM FORMULATION

Let us consider the case of a prolate spheroid in transit near the infinite plane with a protrusion (Figure 2). The spheroid translates with constant speed U in the fore-and-aft direction parallel to the X -axis. The protrusion is a rectangle of length $2d$ and height h , and extends to infinity at both sides. S_1 denotes the surface of the spheroid and $S_i, i = 2, \dots, 5$, are the sub-surfaces of the protrusion defined in Figure 2. The local Cartesian co-ordinates x,y,z are fixed to the spheroid with the origin at the center and the x -, y -, X - and Y -axis in the same vertical plane. The horizontal and vertical separation distances from the center of the spheroid to the origin of the fixed co-ordinates XYZ are L and H , respectively. The main purpose of this study is to simulate the constraining forces and moments acting on the spheroid in such a physical situation. We denote the half length of the major axis of the spheroid by a and its focal distance by c . Let η, θ and φ be the orthogonal confocal co-ordinate system defined by

$$x = c \cosh \eta \cos \theta \quad y = c \sinh \eta \sin \theta \cos \varphi \quad z = c \sinh \eta \sin \theta \sin \varphi, \quad (10)$$

where $0 \leq \theta \leq \pi$ and $0 \leq \varphi \leq 2\pi$. The surfaces where η is a constant are confocal prolate spheroids of revolution with common foci at the points $(\pm c, 0, 0)$. Let η_0 be on surface S_1 . We have

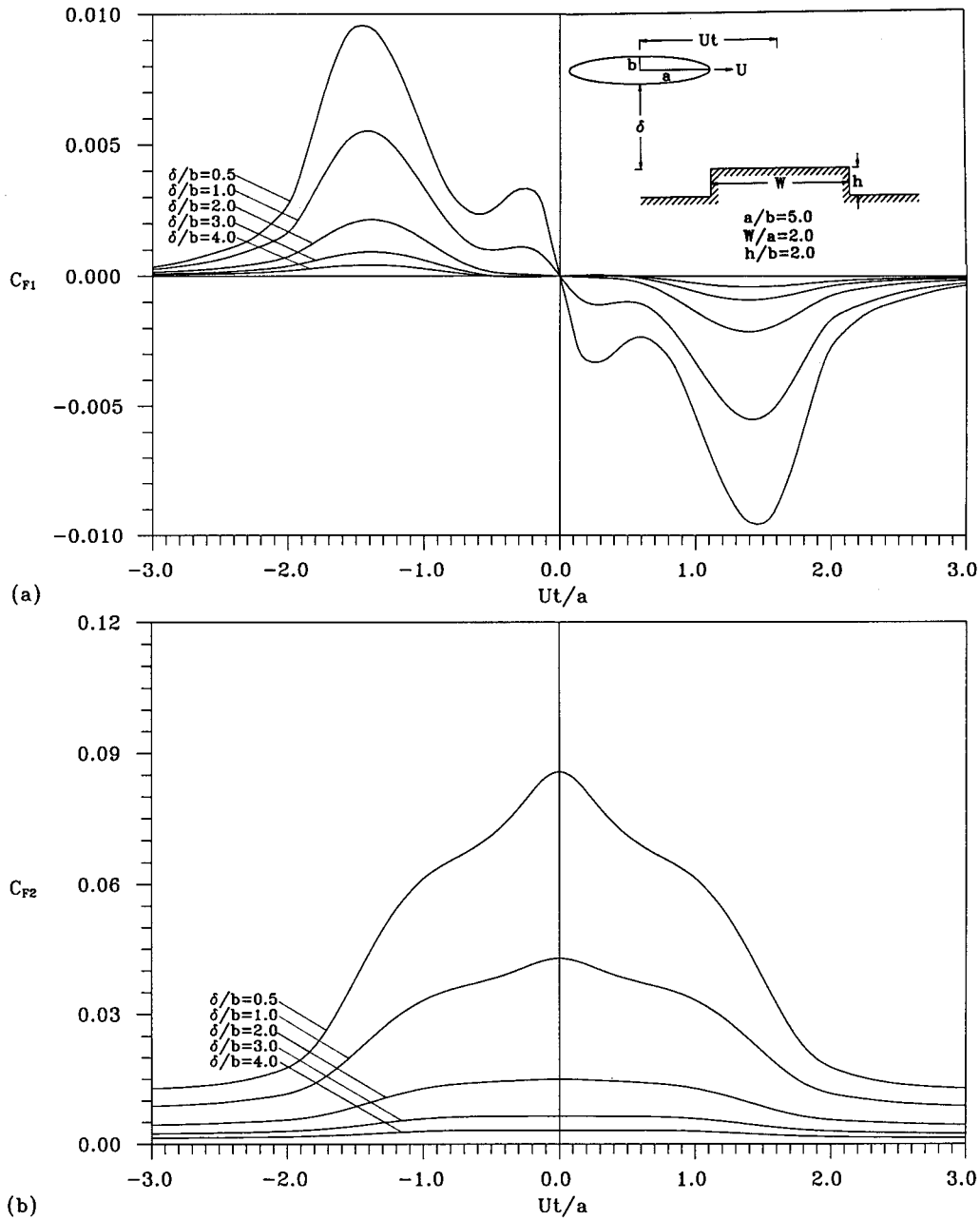


Figure 6. Force and moment coefficients for a spheroid past a platform for varying δ : (a) horizontal force coefficients; (b) vertical force coefficients; (c) moment coefficients.

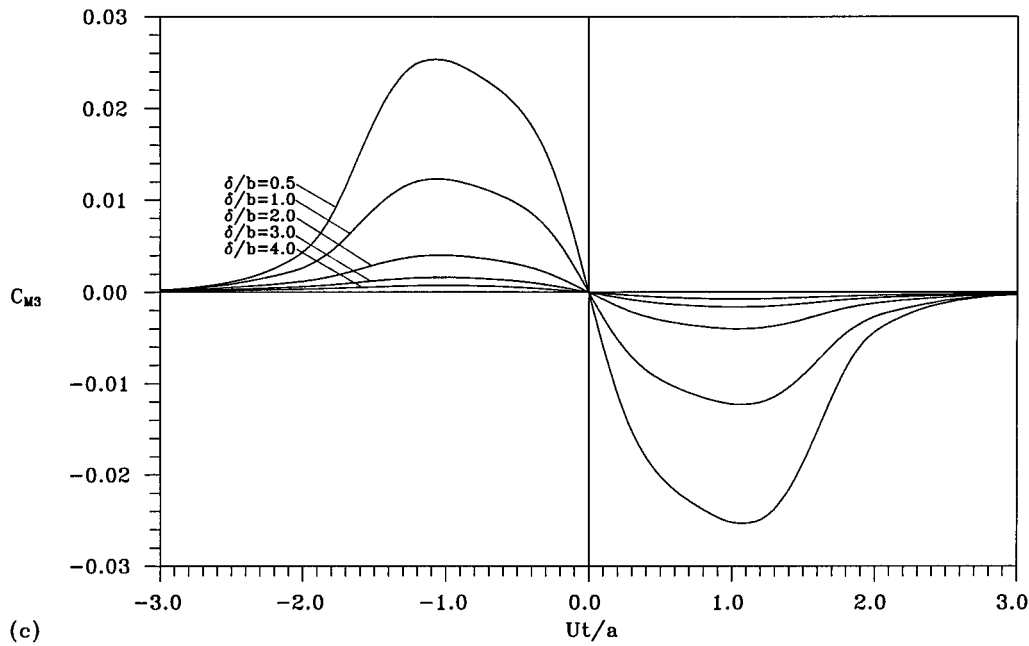


Figure 6 (Continued)

$$a = c \cosh \eta_0, \quad b = c \sinh \eta_0, \tag{11}$$

where b denotes the half length of the minor axis of the spheroid.

The boundary conditions give

$$\frac{\partial \phi}{\partial n} \Big|_{S_1} = U \frac{\partial x}{\partial n} \Big|_{S_1} = \frac{U \sinh \eta_0 \cos \theta}{\sqrt{\cosh^2 \eta_0 - \cos^2 \theta}}, \quad \text{on the spheroid,} \tag{12}$$

and

$$\frac{\partial \phi}{\partial Y}(X, 0, Z) = 0, \tag{13a}$$

$$\frac{\partial \phi}{\partial X}(\pm d, 0, Z) = 0, \quad \text{on the protrusion,} \tag{13b}$$

$$\frac{\partial \phi}{\partial Y}(X, h, Z) = 0. \tag{13c}$$

From the equations of motion (7), we can show that

$$F_1 = \frac{1}{2} \frac{\partial A_1}{\partial L} U^2, \tag{14}$$

$$F_2 = -\frac{1}{2} \frac{\partial A_1}{\partial H} U^2, \tag{15}$$

$$M_3 = -\frac{1}{2} \frac{\partial A_1}{\partial \Omega_3} U^2, \tag{16}$$

where we have made $A_1 = A_{11}$ for convenience. F_1 and F_2 denote the x - and y -components of extraneous force acting on the spheroid through the center, M_3 is the pitch moment, and Ω_3 , the Euler angle, will be defined later. We may define the force and moment coefficients by

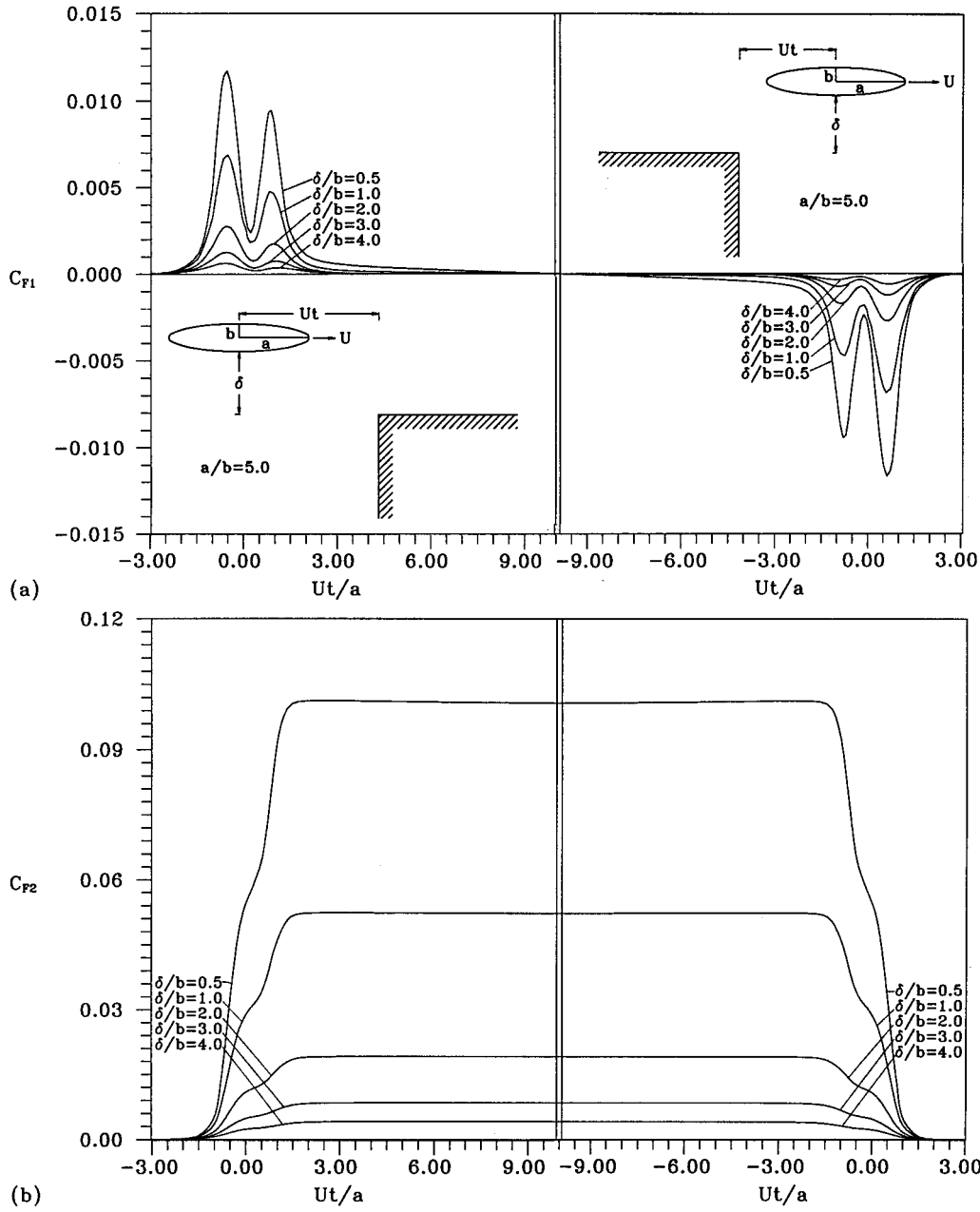


Figure 7. Force and moment coefficients for a spheroid past a huge platform for varying δ : (a) horizontal force coefficients; (b) vertical force coefficients; (c) moment coefficients.

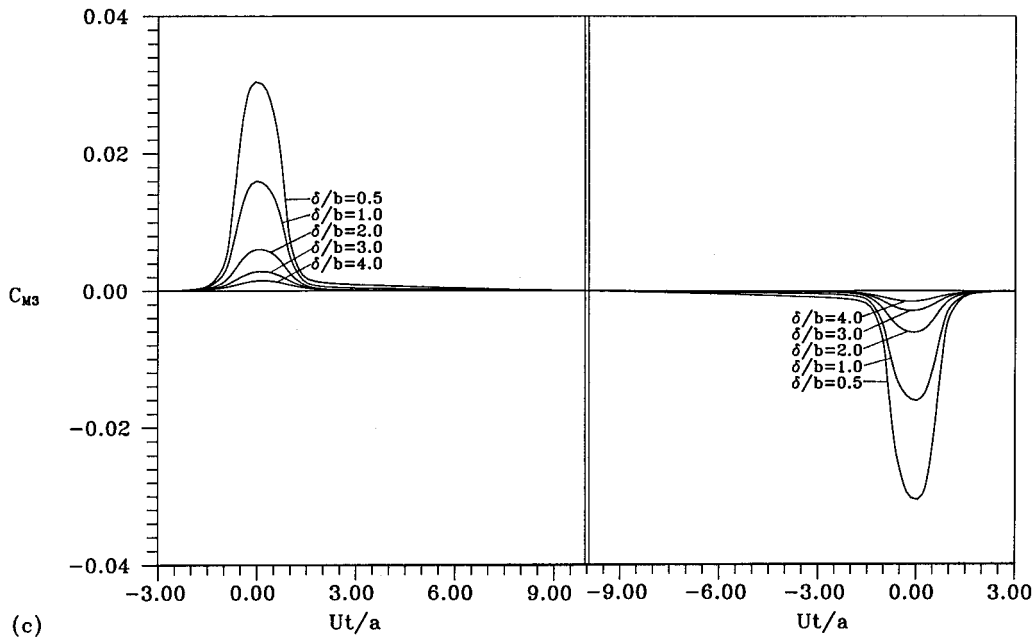


Figure 7 (Continued)

$$C_{F1} = \frac{F_1}{1/2 \rho U^2 \pi b^2}, \tag{17}$$

$$C_{F2} = \frac{F_2}{1/2 \rho U^2 \pi b^2}, \tag{18}$$

$$C_{M3} = \frac{M_3}{1/2 \rho U^2 \pi b^2 a}. \tag{19}$$

The added-mass of the spheroid, A_1 , which is due to a unit velocity in the x direction, can be obtained in terms of the generalized Taylor's formula

$$A_1 = -m' + 4\pi\rho \iint_{S_1} x\sigma_1 dS, \tag{20}$$

where m' denotes the mass of the fluid displaced by the spheroid, and x is the local co-ordinate of the source strength σ_1 . As usually defined in classical mechanics, the Euler angles are independent parameters which serve to carry out the transformation from a given Cartesian co-ordinate system to another. If the spheroid is allowed to rotate, the Euler angles Ω_1 , Ω_2 and Ω_3 are in the xyz -convention, such that the first rotation is the pitch angle Ω_3 about the z axis, the second is the yaw angle Ω_2 about the intermediary y axis, and the third is the roll angle Ω_1 about the final x axis. This allows the relationship between the rotating body co-ordinates xyz and the fixed-space co-ordinates XYZ to be expressed in the following manner [26]:

$$\begin{aligned} X - L &= (\cos \Omega_2 \cos \Omega_3)x + (\sin \Omega_1 \sin \Omega_2 \cos \Omega_3 - \cos \Omega_1 \sin \Omega_3)y \\ &+ (\cos \Omega_1 \sin \Omega_2 \cos \Omega_3 + \sin \Omega_1 \sin \Omega_3)z, \end{aligned} \tag{21a}$$

$$Y - H = (\cos \Omega_2 \sin \Omega_3)x + (\sin \Omega_1 \sin \Omega_2 \sin \Omega_3 + \cos \Omega_1 \cos \Omega_3)y + (\cos \Omega_1 \sin \Omega_2 \sin \Omega_3 - \sin \Omega_1 \cos \Omega_3)z, \tag{21b}$$

$$Z = (-\sin \Omega_2)x + (\cos \Omega_2 \sin \Omega_1)y + (\cos \Omega_2 \cos \Omega_1)z. \tag{21c}$$

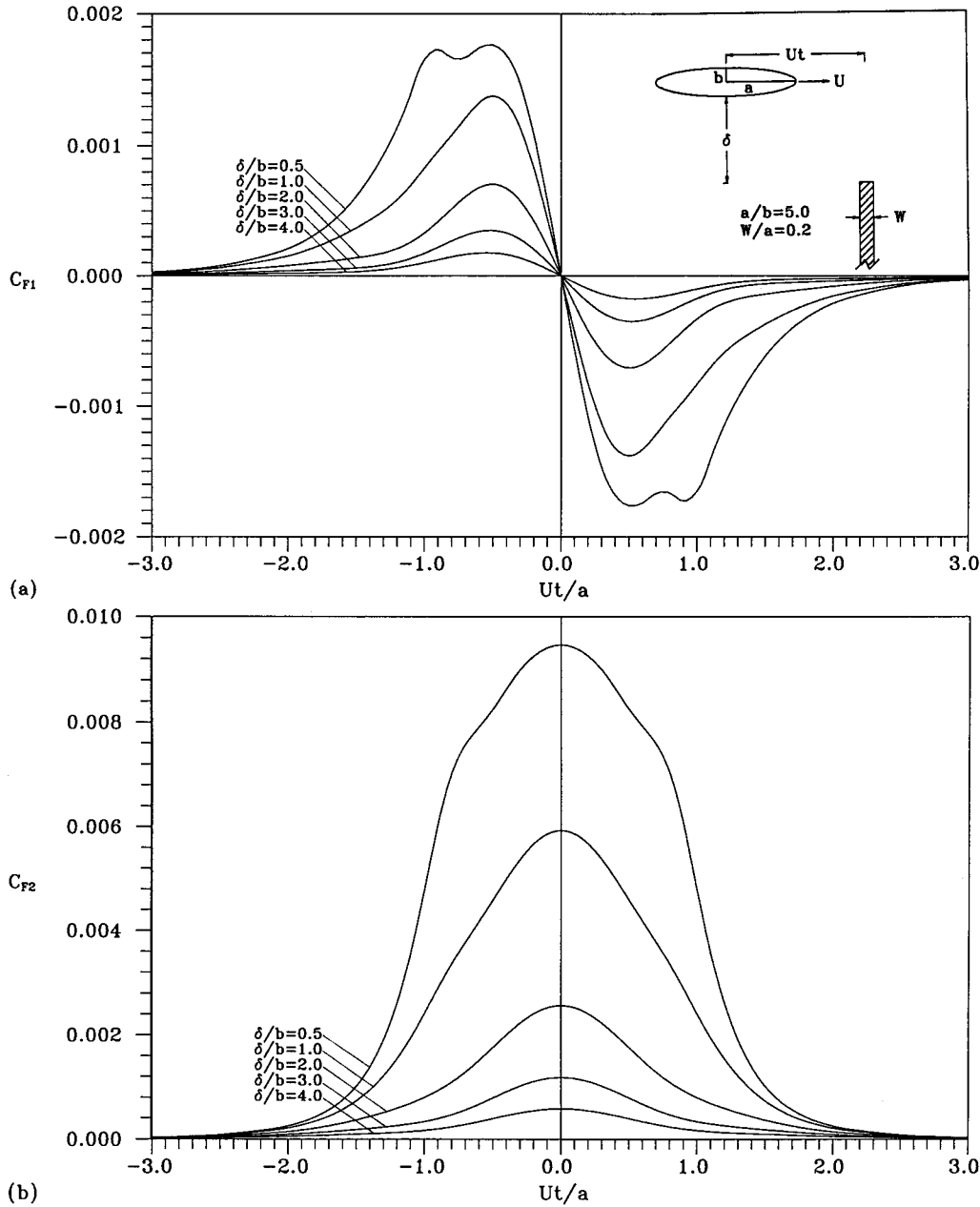


Figure 8. Force and moment coefficients for a spheroid past a thin wall for varying δ : (a) horizontal force coefficients; (b) vertical force coefficients; (c) moment coefficients.

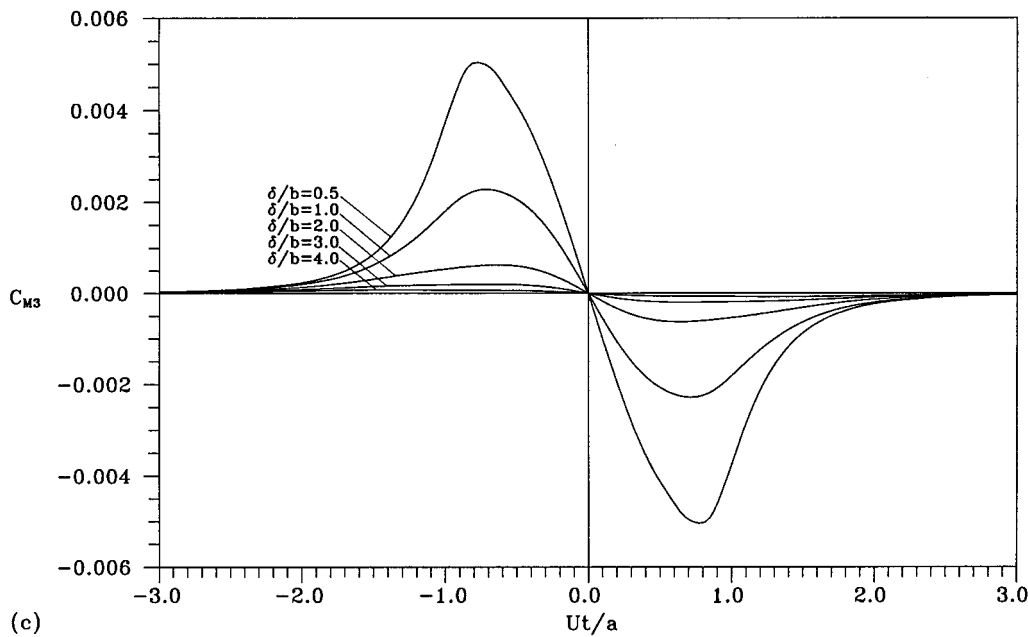


Figure 8 (Continued)

In the present case, however, the Euler angles are simply set to zero.

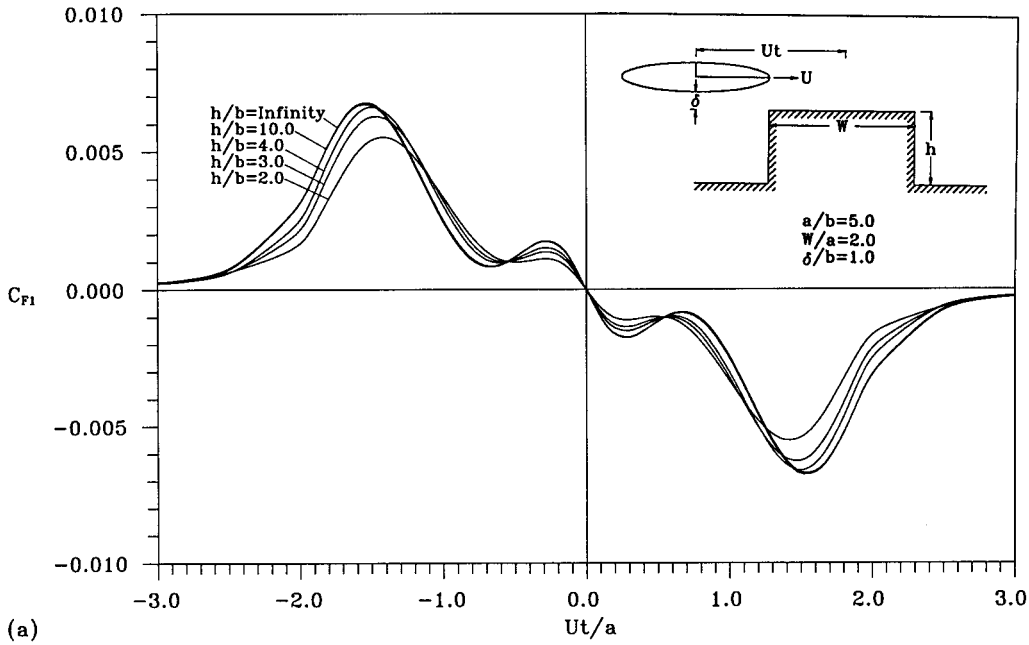
For convenience and clarity, let σ'_i denote the source strength of the field point (X'_i, Y'_i, Z'_i) , and σ_i denote the source strength of the source point (X_i, Y_i, Z_i) on surface S_i . Equation (6) can now be written in the following forms according to the boundary conditions given in (12) and (13):

$$\begin{aligned} \frac{U \sinh \eta_0 \cos \theta'}{\sqrt{\cosh^2 \eta_0 - \cos^2 \theta'}} = & 4\pi\sigma'_1 + \iint_{S_1} (\sigma'_1 D_{11}^* - \sigma_1 D_{11}) dS - \iint_{S_2} \sigma_2 D_{21} dX_2 dZ_2 \\ & - \int_{-\infty}^{\infty} \int_0^h \sigma_3 D_{31} dY_3 dZ_3 - \int_{-\infty}^{\infty} \int_{-d}^d \sigma_4 D_{41} dX_4 dZ_4 \\ & - \int_{-\infty}^{\infty} \int_0^h \sigma_5 D_{51} dY_5 dZ_5, \end{aligned} \tag{22a}$$

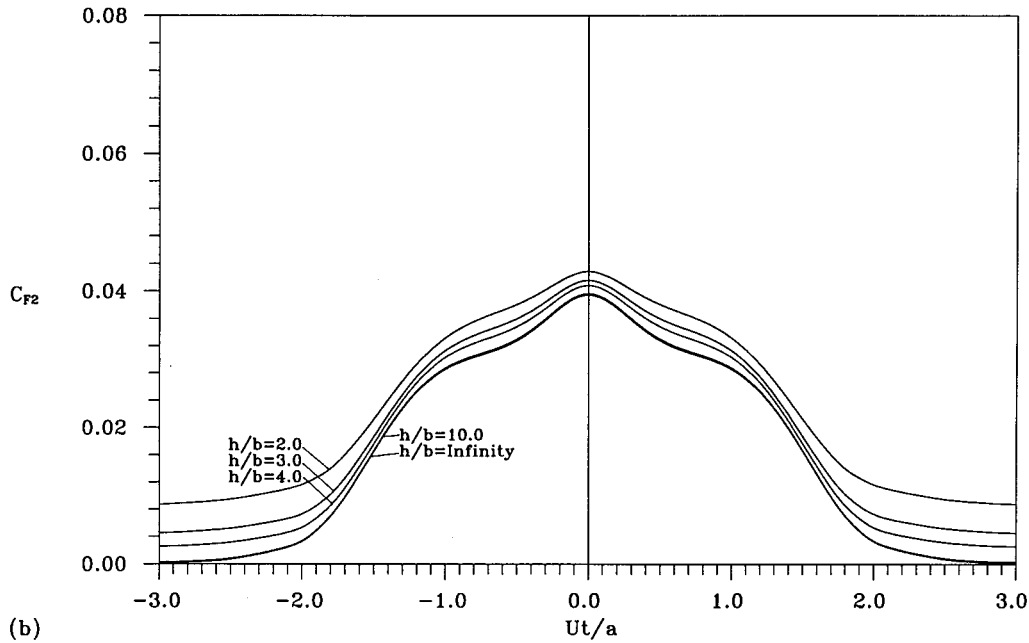
$$\begin{aligned} 0 = & 2\pi\sigma'_2 - \iint_{S_1} \sigma_1 D_{12} dS - \int_{-\infty}^{\infty} \int_0^h \sigma_3 D_{32} dY_3 dZ_3 - \int_{-\infty}^{\infty} \int_{-d}^d \sigma_4 D_{42} dX_4 dZ_4 \\ & - \int_{-\infty}^{\infty} \int_0^h \sigma_5 D_{52} dY_5 dZ_5, \end{aligned} \tag{22b}$$

$$\begin{aligned} 0 = & 2\pi\sigma'_3 - \iint_{S_1} \sigma_1 D_{13} dS - \iint_{S_2} \sigma_2 D_{23} dX_2 dZ_2 - \int_{-\infty}^{\infty} \int_{-d}^d \sigma_4 D_{43} dX_4 dZ_4 \\ & - \int_{-\infty}^{\infty} \int_0^h \sigma_5 D_{53} dY_5 dZ_5, \end{aligned} \tag{22c}$$

$$0 = 2\pi\sigma'_4 - \iint_{S_1} \sigma_1 D_{14} dS - \iint_{S_2} \sigma_2 D_{24} dX_2 dZ_2 - \int_{-\infty}^{\infty} \int_0^h \sigma_3 D_{34} dY_3 dZ_3 - \int_{-\infty}^{\infty} \int_0^h \sigma_5 D_{54} dY_5 dZ_5, \tag{22d}$$



(a)



(b)

Figure 9. Force and moment coefficients for a spheroid past a platform for varying h : (a) horizontal force coefficients; (b) vertical force coefficients; (c) moment coefficients.

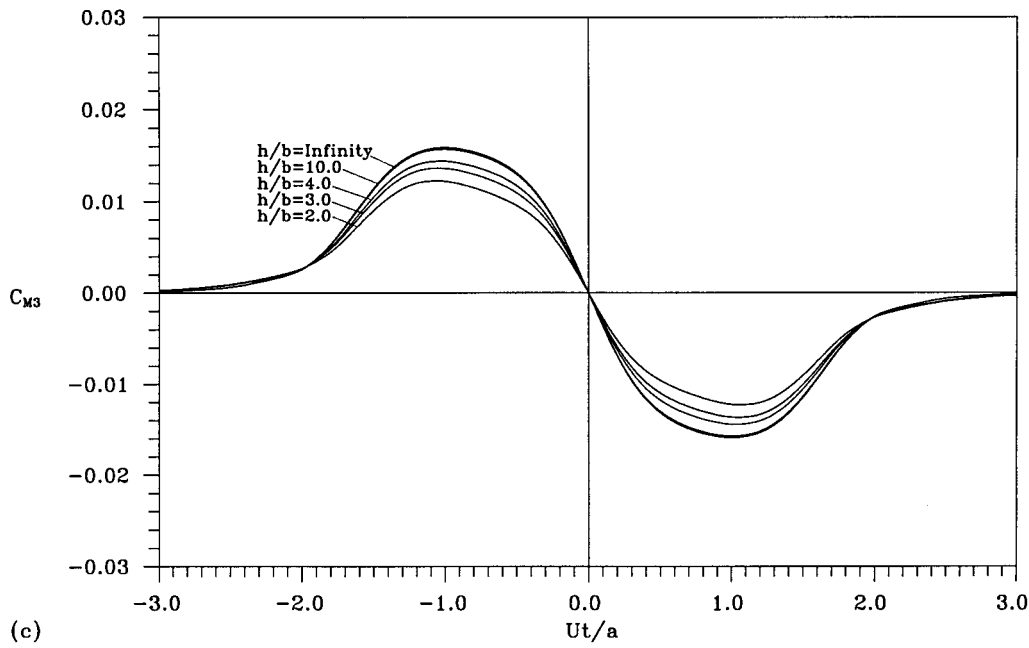


Figure 9 (Continued)

$$0 = -2\pi\sigma'_5 - \iint_{S_1} \sigma_1 D_{15} dS - \iint_{S_2} \sigma_2 D_{25} dX_2 dZ_2 - \int_{-\infty}^{\infty} \int_0^h \sigma_3 D_{35} dY_3 dZ_3 - \int_{-\infty}^{\infty} \int_{-d}^d \sigma_4 D_{45} dX_4 dZ_4. \tag{22e}$$

The element of surface of the spheroid is given by:

$$dS = c^2(\cosh^2 \eta_0 - \cos^2 \theta)^{1/2} \sinh \eta_0 \sin \theta d\theta d\varphi. \tag{23}$$

Let R_{ij} represent the distance from the field point (X'_j, Y'_j, Z'_j) to the source point (X_i, Y_i, Z_i) , where $i, j = 1, 2, \dots, 5$, and can be written as

$$R_{ij} = R(X'_j, Y'_j, Z'_j; X_i, Y_i, Z_i) = \sqrt{(X'_j - X_i)^2 + (Y'_j - Y_i)^2 + (Z'_j - Z_i)^2}, \tag{24}$$

for example,

$$R_{11} = R(X'_1, Y'_1, Z'_1; X_1, Y_1, Z_1) = R(L + x', H + y', z'; L + x, H + y, z) = \sqrt{(x' - x)^2 + (y' - y)^2 + (z' - z)^2}, \tag{24a}$$

$$R_{12} = R(X'_2, Y'_2, Z'_2; X_1, Y_1, Z_1) = R(X'_2, 0, Z'_2; L + x, H + y, z) = \sqrt{(X'_2 - L - x)^2 + (H + y)^2 + (Z'_2 - z)^2}. \tag{24b}$$

For convenience, we also write $\partial/\partial n_i = \partial/\partial n_p$ and $\partial/\partial n'_i = \partial/\partial n_Q$ on surface S_i . D_{11}^* is then defined by

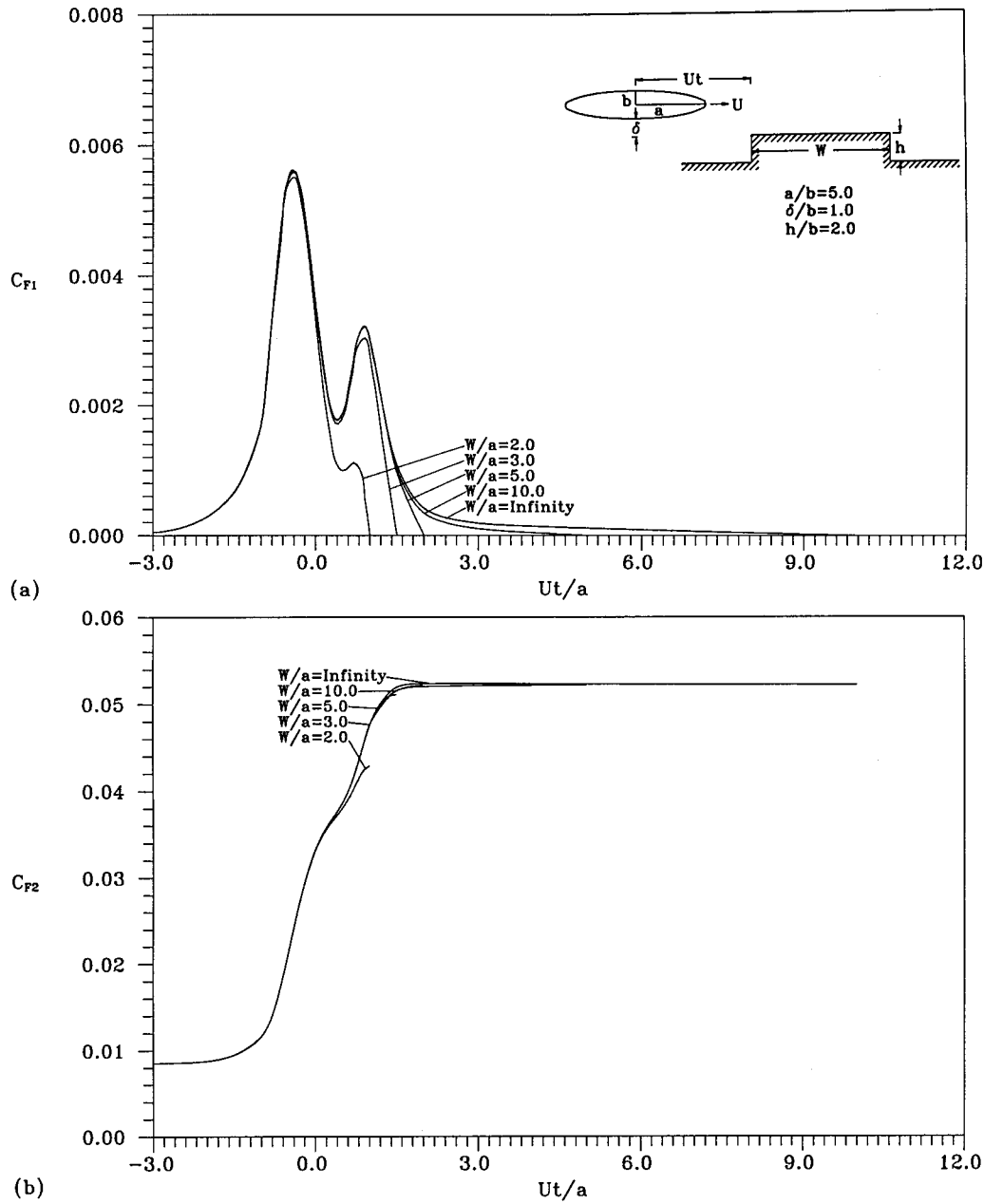


Figure 10. Force and moment coefficients for a spheroid past a platform for varying W : (a) horizontal force coefficients; (b) vertical force coefficients; (c) moment coefficients.

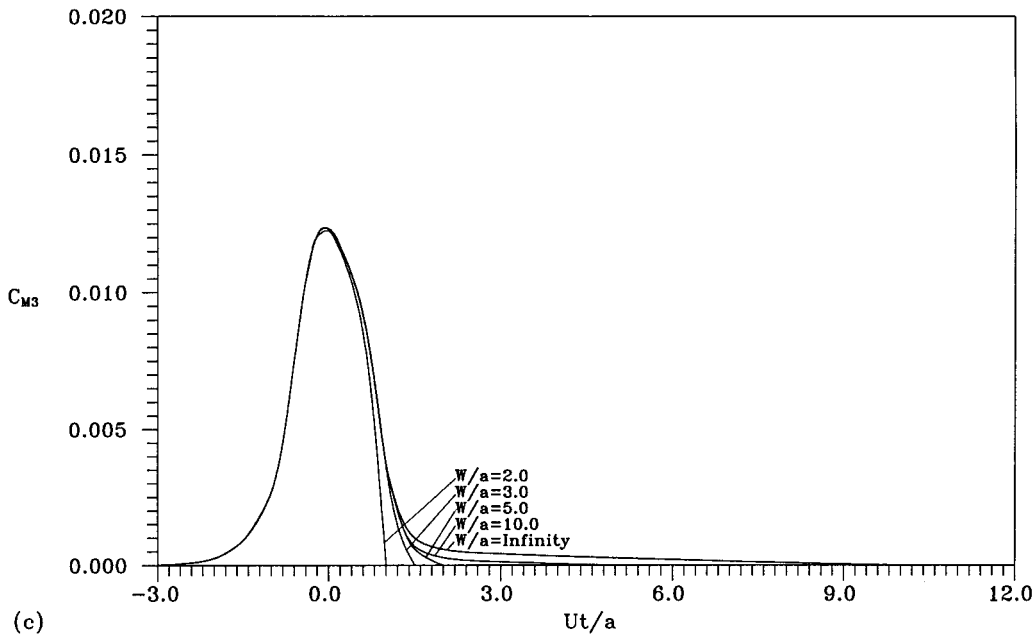


Figure 10 (Continued)

$$\begin{aligned}
 D_{11}^* &= \frac{\partial}{\partial n_1} \left(\frac{1}{R_{11}} \right) = \frac{\partial}{\partial \eta} \left(\frac{1}{R_{11}} \right) \frac{1}{c \sqrt{\cosh^2 \eta_0 - \cos^2 \theta}} \\
 &= -c \frac{\cosh \eta_0 \sinh \eta_0}{\sqrt{\cosh^2 \eta_0 - \cos^2 \theta}} \frac{1 - \cos \theta \cos \theta' - \sin \theta \sin \theta' \cos(\varphi - \varphi')}{R_{11}^3}, \tag{25}
 \end{aligned}$$

and D_{ij} , where $i, j = 1, \dots, 5$, is defined by

$$D_{ij} = \frac{\partial}{\partial n'_j} \left(\frac{1}{R_{ij}} \right). \tag{26}$$

If $i = 1$ and $j = 1$, then

$$D_{11} = \frac{\partial}{\partial n'_1} \left(\frac{1}{R_{11}} \right) = -c \frac{\cosh \eta_0 \sinh \eta_0}{\sqrt{\cosh^2 \eta_0 - \cos^2 \theta'}} \frac{1 - \cos \theta \cos \theta' - \sin \theta \sin \theta' \cos(\varphi - \varphi')}{R_{11}^3}, \tag{27}$$

otherwise,

$$D_{ij} = D_j(X'_j, Y'_j, Z'_j; X_i, Y_i, Z_i), \tag{28}$$

where

$$D_1(X'_1, Y'_1, Z'_1; X_i, Y_i, Z_i) = -\frac{B_i}{R_{i1}^3} \frac{1}{\sqrt{\cosh^2 \eta_0 - \cos^2 \theta'}}, \tag{28a}$$

$$D_2(X'_2, Y'_2, Z'_2; X_i, Y_i, Z_i) = \frac{Y_i}{R_{i2}^3}, \tag{28b}$$

$$D_3(X'_3, Y'_3, Z'_3; X_i, Y_i, Z_i) = -\frac{d - X_i}{R_{i3}^3}, \tag{28c}$$

$$D_4(X'_4, Y'_4, Z'_4; X_i, Y_i, Z_i) = -\frac{h - Y_i}{R_{i4}^3}, \tag{28d}$$

$$D_5(X'_5, Y'_5, Z'_5; X_i, Y_i, Z_i) = \frac{d + X_i}{R_{i5}^3}, \tag{28e}$$

and where

$$B_i = (L - X_i) \sinh \eta_0 \cos \theta' + (H \cos \varphi' - Y_i \cos \varphi' - Z_i \sin \varphi') \cosh \eta_0 \sin \theta' + c \cosh \eta_0 \sinh \eta_0, \tag{29}$$

for example,

$$B_2 = (L - X_2) \sinh \eta_0 \cos \theta' + (H \cos \varphi' - Z_2 \sin \varphi') \cosh \eta_0 \sin \theta' + c \cosh \eta_0 \sinh \eta_0, \tag{29a}$$

$$B_4 = (L - X_4) \sinh \eta_0 \cos \theta' + (H \cos \varphi' - h \cos \varphi' - Z_4 \sin \varphi') \cosh \eta_0 \sin \theta' + c \cosh \eta_0 \sinh \eta_0. \tag{29b}$$

In the numerical computation, we discretized (22a)–(22e) by the Gauss–Legendre quadrature formula and calculated the source distribution by the Gauss–Seidel iterative method.

To find the force and moment coefficients, we need to evaluate the derivatives of added-mass. From (20), we have

$$\frac{\partial A_1}{\partial L} = 4\pi\rho \iint_{S_1} x \frac{\partial \sigma_1}{\partial L} dS, \tag{30}$$

$$\frac{\partial A_1}{\partial H} = 4\pi\rho \iint_{S_1} x \frac{\partial \sigma_1}{\partial H} dS, \tag{31}$$

$$\frac{\partial A_1}{\partial \Omega_3} = 4\pi\rho \iint_{S_1} x \frac{\partial \sigma_1}{\partial \Omega_3} dS, \tag{32}$$

where $\partial \sigma_1 / \partial L$, $\partial \sigma_1 / \partial H$ and $\partial \sigma_1 / \partial \Omega_3$ are obtained from (22a)–(22e) by taking derivatives with respect to L , H and Ω_3 , respectively. Consequently, we have to solve three sets of integral equations for two components of the force and the pitch moment. We list the first set in the following:

$$0 = 4\pi \frac{\partial \sigma'_1}{\partial L} + \iint_{S_1} \left(\frac{\partial \sigma'_1}{\partial L} D_{11}^* - \frac{\partial \sigma_1}{\partial L} D_{11} \right) dS - \iint_{S_2} \left(\frac{\partial \sigma_2}{\partial L} D_{21} + \sigma_2 \frac{\partial D_{21}}{\partial L} \right) dX_2 dZ_2 - \int_{-\infty}^{\infty} \int_0^h \left(\frac{\partial \sigma_3}{\partial L} D_{31} + \sigma_3 \frac{\partial D_{31}}{\partial L} \right) dY_3 dZ_3 - \int_{-\infty}^{\infty} \int_{-d}^d \left(\frac{\partial \sigma_4}{\partial L} D_{41} + \sigma_4 \frac{\partial D_{41}}{\partial L} \right) dX_4 dZ_4 - \int_{-\infty}^{\infty} \int_0^h \left(\frac{\partial \sigma_5}{\partial L} D_{51} + \sigma_5 \frac{\partial D_{51}}{\partial L} \right) dY_5 dZ_5, \tag{33a}$$

$$0 = 2\pi \frac{\partial \sigma'_2}{\partial L} - \iint_{S_1} \left(\frac{\partial \sigma_1}{\partial L} D_{12} + \sigma_1 \frac{\partial D_{12}}{\partial L} \right) dS - \int_{-\infty}^{\infty} \int_0^h \frac{\partial \sigma_3}{\partial L} D_{32} dY_3 dZ_3 - \int_{-\infty}^{\infty} \int_{-d}^d \frac{\partial \sigma_4}{\partial L} D_{42} dX_4 dZ_4 - \int_{-\infty}^{\infty} \int_0^h \frac{\partial \sigma_5}{\partial L} D_{52} dY_5 dZ_5, \tag{33b}$$

$$0 = 2\pi \frac{\partial \sigma'_3}{\partial L} - \iint_{S_1} \left(\frac{\partial \sigma_1}{\partial L} D_{13} + \sigma_1 \frac{\partial D_{13}}{\partial L} \right) dS - \iint_{S_2} \frac{\partial \sigma_2}{\partial L} D_{23} dX_2 dZ_2 - \int_{-\infty}^{\infty} \int_{-d}^d \frac{\partial \sigma_4}{\partial L} D_{43} dX_4 dZ_4 - \int_{-\infty}^{\infty} \int_0^h \frac{\partial \sigma_5}{\partial L} D_{53} dY_5 dZ_5, \quad (33c)$$

$$0 = 2\pi \frac{\partial \sigma'_4}{\partial L} - \iint_{S_1} \left(\frac{\partial \sigma_1}{\partial L} D_{14} + \sigma_1 \frac{\partial D_{14}}{\partial L} \right) dS - \iint_{S_2} \frac{\partial \sigma_2}{\partial L} D_{24} dX_2 dZ_2 - \int_{-\infty}^{\infty} \int_0^h \frac{\partial \sigma_3}{\partial L} D_{34} dY_3 dZ_3 - \int_{-\infty}^{\infty} \int_0^h \frac{\partial \sigma_5}{\partial L} D_{54} dY_5 dZ_5, \quad (33d)$$

$$0 = -2\pi \frac{\partial \sigma'_5}{\partial L} - \iint_{S_1} \left(\frac{\partial \sigma_1}{\partial L} D_{15} + \sigma_1 \frac{\partial D_{15}}{\partial L} \right) dS - \iint_{S_2} \frac{\partial \sigma_2}{\partial L} D_{25} dX_2 dZ_2 - \int_{-\infty}^{\infty} \int_0^h \frac{\partial \sigma_3}{\partial L} D_{35} dY_3 dZ_3 - \int_{-\infty}^{\infty} \int_{-d}^d \frac{\partial \sigma_4}{\partial L} D_{45} dY_4 dZ_4, \quad (33e)$$

where the source strengths have been solved previously in (22a)–(22e). The other two sets of equations can be manipulated in a similar manner and will not be listed here. However, it is noteworthy that (21a)–(21c) have been used to solve $\partial \sigma_1 / \partial \Omega_3$. Again, these equations were discretized by Gauss–Legendre quadrature formula and the unknowns were calculated using the Gauss–Seidel iterative method.

The validity of the present method and corresponding numerical program was checked in Figures 3 and 4 for the problems of a sphere with radius a moving perpendicular and parallel for a fixed plane boundary, respectively. The analytical data of added-mass coefficients and their derivatives were provided by Guo and Chwang [21], and Landweber and Shahshahan [27]. The added-mass coefficient k is defined by the added-mass divided by the mass of the same volume of fluid. The grid distribution on the sphere was set to 20×40 in θ and φ axes. The grid distribution on the plane wall was set to 40×40 for $0 \leq x \leq 5a$ and $-5a \leq x \leq 0$, and similarly for $-5a \leq z \leq 5a$. In Figure 5, we compared the added-mass coefficients of a prolate spheroid moving axially near a plane wall with that obtained by the method of expansion of harmonic functions developed by Farrell [28]. The grid distribution on the spheroid was set to 30×40 in θ and φ axes and the grid distribution on the plane wall was the same as that in the previous case. The comparisons in Figures 3–5 show the preliminary success of the proposed method.

4. NUMERICAL RESULTS

We are now in a position to investigate the core subject, the extraneous forces and moments acting on a prolate spheroid under the circumstances considered. The ratio of length to mid-section diameter, a/b , of the spheroid was set at 5.0. The grid distribution on the spheroid was 30×40 in θ and φ axes, respectively, in all study cases. The grid points on the protrusion depend on the size itself and the relative position of the protrusion to the spheroid. However, we found that, in general, the grid distribution should be denser in the region where the distance between the protrusion and the spheroid is shortest, especially when the spheroid is moving very close to the protrusion. In other words, we divided the surface of the protrusion into several sub-regions and put different grid points in them. This procedure is important, not only for greater accuracy, but also for the convergence of the results. All calculations were carried out on the HP-Apollo 730 Workstation. About 15 iterations for each time step were required to obtain an absolute accuracy of 10^{-6} for the source strength. The grid points for

the strength magnitude of less than 10^{-6} were discarded when improper integrations were encountered in (22a)–(22e). We also found numerically that the accuracy of the derivatives of the source is $\approx 10^{-5}$ in the present case.

Figure 6(a) shows the coefficients of horizontal force for the spheroid moving from left to right for five cruising heights, or five separation distances, $\delta/b = 0.5, 1.0, 2.0, 3.0, 4.0$. The protrusion, which we took at a comparable size to the spheroid, measures $w/a = 2$ in length, where $w = 2d$, and $h/b = 2.0$ in height. The spheroid experiences a resistance force as it approaches the protrusion and a pushing force as it leaves. As to be expected, the magnitude of resistance increases when the body is approaching the step, and the smaller the clearance is, the larger the resistance becomes. It is of interest to note that the smaller peak at $Ut/a \approx \pm 0.2$ becomes more significant for the smaller clearance. The larger first peak value indicates that the spheroid requires increased force to overcome the effect of the presence of the protrusion at the initial stage for retaining constant speed. Figure 6(b) plots the variation of vertical force for several cruising heights. There is a greater, faster increase in force as the body approaches the protrusion for smaller values of clearance. For example, the force increases about seven times as the body moving from $Ut/a = -3.0$ to 0 for $\delta/b = 0.5$, but only about two times for $\delta/b = 4.0$. Figure 6(c) shows the variation of extraneous moment of the spheroid. There exists a constraining counterclockwise moment in the approaching region and a clockwise moment in the leaving region.

Two limiting cases were considered next and the results are shown in Figures 7 and 8. The first one is the case of a spheroid past a huge protrusion. In Figure 7 the left half is for the approaching case and the right half for the leaving case. Examination of Figure 6(a) and Figure 7(a) shows that the magnitude of the original smaller peak increases remarkably and is comparable with the larger peak. In practical applications this phenomenon indicates that the crew may sense two violent shakes in a short distance when the submersibles are approaching or leaving the sea-bed with a huge protrusion, and the clearance is small. Figure 7(b) reveals that the moving body begins to experience an attractive force when the center of the body is at a position which is one body length ahead of the protrusion, then the force reaches the limiting value within a distance of two body lengths. Figure 7(c) shows that the maximum moment occurs when the body is at the top of the corner of the protrusion. Figure 7 exhibits clearly that disaster may befall the submersibles moving very close to a huge protrusion, due to the sudden change in the extraneous forces and moment over a very short distance, only two body lengths in the present case. The second limiting case is the problem of a body approaching a thin wall, such as a breakwater for practical considerations. Figure 8 displays the force and moment coefficients for $w/a = 0.2$ and several clearances. The magnitudes of force and moment coefficients are reduced to $\approx 1/10$ of that in Figure 7. It seems like that the hydrodynamic effects of a thin wall on the body are not so significant as that of a huge protrusion.

Finally, we studied the effects of the size of the protrusion on the moving body. The clearance was kept at $\delta/b = 1$. In Figure 9 the length of the protrusion was set at $w/a = 2$, and five heights ranging from $h/b = 2$ to ∞ were considered. It can be observed from Figure 9(a)–Figure 9(c) that the curves for $h/b = 10$ almost coincide with the curves for $h/b = \infty$. This indicates that the body obtains a limiting influence from a protrusion which has a height five times the diameter of the mid-section of the body. Figure 9(a) also shows that the peak resistance not only increases, but also occurs earlier in the approaching region, and delays in the leaving region when the height of the protrusion increases. In Figure 10 the height of the protrusion was kept at $h/b = 2$ and several lengths were considered. The curves were plotted only for the approaching region in this case. Figure 10(a) shows that the first peak resistance for $w/a = 2$ almost reaches the limiting value, as does the second peak resistance for $w/a = 5$.

It is shown in Figure 10(b) and Figure 10(c) that the vertical force and moment reach the limiting values for $w/a = 5$ and $w/a = 3$, respectively.

5. DISCUSSION AND CONCLUSIONS

In this paper, we have presented the mathematical formulation for the unsteady ground-effect problem under the framework of the Lagrange's equation of motion in connection with the generalized Taylor's formula. Application of the formulation has been depicted in detail using a test example. The boundary-integral method was adopted and the original singular integral equation was regularized, which is of importance for the numerical implementation. The unknowns, source strengths and their derivatives, were solved numerically in terms of the Gauss–Legendre quadrature formula and the iterative method.

The efficacy of the proposed method has been examined using a sphere moving perpendicular and parallel to a plane wall, respectively; and a prolate spheroid moving parallel to a plane wall. The computed added-mass coefficients and their derivatives have been compared with the theoretical solutions. Thereafter, the hydrodynamic interactions between a moving spheroid and a plane wall with a protrusion have been investigated systematically. Several factors which influence the interaction effects have been studied, such as the clearance and the size of the protrusion. A general understanding of the physical problem considered has been obtained from the variations of the horizontal resistance, the vertical force and the pitch moment, and may extend the results to some engineering applications, for example the motion of submersibles in the proximity of the seabed. The first result, which is an obvious one, is that the smaller clearance induces more significant effects on the spheroid. Secondly, for the case of a huge protrusion, the magnitudes of the force and moment coefficients are about ten times greater than in the case of a thin wall. For a constant length and varied height of the protrusion, the corresponding interactions reach the limiting values at a height about five times the diameter of the mid-section of the spheroid. On the contrary, for a constant height and varied length, the limiting values occur at a length about three times of the body length. For a body approaching a huge protrusion, the results show that the body experiences two shakes in the direction of the major axis, due to two peak values of the resistance, a vertical attractive force, and a bow-in moment in the short distance of about two body lengths. This phenomenon is more significant for the body moving closer to the protrusion. Therefore, the precautions of the crew may avoid the possible calamity for submarines cruising in the region near the seabed.

Regardless of the slender-body assumption mentioned in the introduction, in general there are three solution methods for the dynamic effects due to the unsteady motion of one body, or multiple bodies through an inviscid and incompressible fluid. The first is the Lagrange's equation of motion, which expresses the forces and moments in terms of added masses and their derivatives. The second is an application of the unsteady Bernoulli equation, which expresses the forces and moments by integrating the pressure over the body surfaces; and third, initiated by Lagally, expresses the forces and moments in terms of singularities and gradients of velocity potential. The first solution method was adopted in the present study. The second method yields the expression of the i th force component acting on the moving body with surface S in the form

$$F_i = \iint_S P n_i \, dS = -\rho \iint_S \left(\frac{\partial \phi}{\partial t} + \frac{1}{2} \nabla \phi \cdot \nabla \phi \right) n_i \, dS. \quad (34)$$

A major difficulty with equation (34) is the calculation of the unsteady term, because the body is in motion. Some methods have been proposed to surmount the nuisance [29,30]. For an easier numerical calculation (34) can be rewritten as

$$F_i = -\rho \frac{d}{dt} \iint_S \phi n_i dS + \rho \iint_S \left(\frac{\partial \phi}{\partial n} u_i - \frac{1}{2} \nabla \phi \cdot \nabla \phi n_i \right) dS, \tag{35}$$

where $\vec{u} = \nabla \phi$. The unsteady Lagally theory [31,32] yields the expression of the *i*th force component acting on the moving body at a constant speed in the following:

$$F_i = -4\pi\rho \left(\frac{d}{dt} \iint_S \sigma x_i dS + \iint_S \sigma u_i dS \right). \tag{36}$$

We can now compare the expressions in (14), (15), (35) and (36) for the three alternative methods. Application of the Lagrange’s formulation requires the added masses and their derivatives, or singularity strengths and their derivatives to be solved after applying Taylor’s formula. For the method of pressure integration, the velocity potential and the corresponding derivative with respect to time, and the velocity vector $\nabla \phi$ on the body surface must be solved. As regards the Lagally theory, equation (36) shows that the singularity strengths and the corresponding time derivatives, and the velocity vector must be solved. It seems that the Lagrange’s formulation is more convenient for the numerical implementation, especially based on the regularized integral equations which facilitate the direct use of quadrature formulas. The regularization technique demonstrated in Section 2 can also be applied to the methods of the Bernoulli equation and Lagally theory with one exception, that the computation of the velocity vector requires particular care in view of the Cauchy singularity in the kernel [33]. Since the corresponding Cauchy singularity can not be removed at the present stage, the merit of the direct use of quadrature formulas is then lost. In view of this fact, no attempt was made to repeat the numerical simulation using the latter two methods.

Theoretically, the algorithm developed in the present study could be extended to treat more general motion of a body (or bodies) in more complex environments. It is known, however, that most of the computing time for the numerical implementation is expended on setting up the matrix itself, not solving it, after the integral equations are discretized into a linear system of algebraic equations. Some other efficient algorithms for reducing the computational burden and storage are then required, particularly for multiple-body interaction problems. The global methods, which define the unknown functions globally as smooth functions on the integration domain, for example the Chebyshev polynomials, may be one solution [34,35]. Instead of solving the unknown functions directly, we are computing the coefficients in the function expansions. Finally, it is worth noting that the potential flow theory provides the first-order approximation of the hydrodynamic effects, as mentioned in the introduction, providing the moving body is not very close to the obstacles. The exact region of validity of the theory could be quantified by the experiments. It is recognized however that the flow data around a moving body may not be obtained easily. Particular attention should be paid to the relevant experimental procedures [36].

ACKNOWLEDGMENTS

The authors wish to thank the National Science Council, Republic of China, for their financial support under grant No. NSC 81-0403-E-006-559. The acknowledgement is also extended to Mr. B.-F. Cheng and Mr. C.-C. Chieu for programming assistance.

APPENDIX A. NOMENCLATURE

The following symbols are used in this paper:

A_{ij}	added masses
a	half length of the major axis of the spheroid
b	half length of the minor axis of the spheroid
c	focal distance of the spheroid
d	half length of the protrusion
H	vertical separation distance from the center of the spheroid to the origin of the fixed co-ordinates XYZ
L	horizontal separation distance from the center of the spheroid to the origin of the fixed co-ordinates XYZ
m	mass of the moving body
m'	mass of the fluid displaced by the moving body
n	outward normal at the body surface
n_i	i th component of the outward normal n
P	source point
Q	field point
Q_i	generalized forces
q_i	generalized co-ordinates
\dot{q}_i	generalized velocities
R	distance between the field point and the source point
S_1, S_2	surfaces of body 1 or 2
T	total kinetic energy
t	time co-ordinate
U_i	i th velocity component of the moving body
w	length of the protrusion
X, Y, Z	fixed-space Cartesian co-ordinates
x_1, y_1, z_1	Cartesian co-ordinates fixed in body 1
δ_{ij}	Kronecker delta
η, θ, φ	orthogonal confocal co-ordinate system
ρ	density of the fluid
σ	surface source distribution
ϕ	velocity potential
ϕ_i	velocity potential corresponding to $U_i = 1$ and other velocity components are zero
Ω_i	Euler angles
∇^2	Laplacian operator

REFERENCES

1. W.M. Hicks, 'On the motion of two cylinders in a fluid', *Quart. J. Math.* **XVI**, 113–140, 193–219 (1879).
2. W.M. Hicks, 'On the motion of two spheres in a fluid', *Philosophical Transactions*, Royal Society of London, **171**, 455–492 (1880).
3. T.H. Havelock, 'Wave resistance: the mutual action of two bodies', *Proc. Roy. Soc. London Ser. A*, **155**, 460–471 (1936).

4. E.O. Tuck, 'A systematic asymptotic expansion procedure for slender ships', *J. Ship Res.*, **8**, 15–23 (1964).
5. E.O. Tuck, 'Shallow-water flows past slender bodies', *J. Fluid Mech.*, **26**, 81–95 (1966).
6. J.N. Newman, 'Lateral motion of a slender body between two parallel walls', *J. Fluid Mech.*, **39**, 97–115 (1969).
7. E.O. Tuck and J.N. Newman, 'Hydrodynamic interactions between ships', *Proceedings, Tenth Symposium on Naval Hydrodynamics*, Cambridge, MA, 1974.
8. S. Wang, 'Dynamic effects of ship passage on moored vessels', *J. Waterways, Harbors, and Coastal Engrg. Div., Proc. ASCE*, **101**, 247–258 (1975).
9. G.W. King, 'Unsteady hydrodynamic interactions between ships', *J. Ship Res.*, **21**, 157–164 (1977).
10. R.W. Yeung and W.Y. Hwang, 'Nearfield hydrodynamic interactions of ships in shallow water', *J. Hydraulics*, **11**, 128–135 (1977).
11. R.W. Yeung, 'On the interactions of slender ships in shallow water', *J. Fluid Mech.*, **85**, 143–159 (1978).
12. F. Hess, 'Lateral forces on a ship approaching a vertical wall: a theoretical model', *J. Ship Res.*, **23**, 284–296 (1979).
13. R.W. Yeung and W.T. Tan, 'Hydrodynamic interactions of ships with fixed obstacles', *J. Ship Res.*, **24**, 50–59 (1980).
14. A.M.J. Davis and J.F. Geer, 'The application of uniform-slender-body theory to the motion of two ships in shallow water', *J. Fluid Mech.*, **114**, 419–441 (1982).
15. A.M.J. Davis, 'Hydrodynamic effects of fixed obstacles on ships in shallow water', *J. Ship Res.*, **30**, 94–102 (1986).
16. S.K. Chow, A.Y. Hou and L. Landweber, 'Hydrodynamic forces and moments acting on a body emerging from an infinite plane', *Phys. Fluids*, **19**, 1439–1449 (1976).
17. T. Miloh and L. Landweber, 'Generalization of the Kelvin–Kirchhoff equations for the motion of a body through a fluid', *Phys. Fluids*, **24**, 6–9 (1981).
18. L. Landweber and A.T. Chwang, 'Generalization of Taylor's added-mass formula for two bodies', *J. Ship Res.*, **33**, 1–9 (1989).
19. L. Landweber, A.T. Chwang and Z. Guo, 'Interaction between two bodies translating in an inviscid fluid', *J. Ship Res.*, **35**, 1–8 (1991).
20. Z. Guo and A.T. Chwang, 'Oblique impact of two cylinders in a uniform flow', *J. Ship Res.*, **35**, 219–229 (1991).
21. Z. Guo and A.T. Chwang, 'On the planar translation of two bodies in a uniform flow', *J. Ship Res.*, **36**, 38–54 (1992).
22. T. Miloh and A. Hauptman, 'Large-amplitude motion of an elongated body in shallow water', *J. Ship Res.*, **24**, 256–270 (1980).
23. T. Miloh, 'Hamilton's principle, Lagrange's method, and ship motion theory', *J. Ship Res.*, **28**, 229–237 (1984).
24. G.A. Athanassoulis and T.A. Loukakis, 'Lagrangian expressions of the hydrodynamic forces acting on a rigid body in the presence of a free surface', *J. Ship Res.*, **29**, 12–22 (1985).
25. H. Lamb, *Hydrodynamics*, 6th edn, Chapter 6, Cambridge University Press, Cambridge, UK, 1932.
26. H. Goldstein, *Classical Mechanics*, 2nd edn, Appendix B, Addison-Wesley, Reading, MA, 1980.
27. L. Landweber and A. Shahshahan, *Added Masses and Forces on Two Bodies Approaching Central Impact in an Inviscid Fluid*, IIHR Rep. No. 346, Iowa Institute of Hydraulic Research, The University of Iowa, Iowa, 1991.
28. C. Farell, 'On the flow about a spheroid near a plane wall', *J. Ship Res.*, **15**, 246–252 (1971).
29. J.N. Newman, *Marine Hydrodynamics*, Section 4.12, MIT Press, Cambridge, MA, 1977.
30. K. Kikuchi, T. Maeda and M. Yanagizawa, 'Numerical simulation of the phenomena due to the passing-by of two bodies using the unsteady boundary element method', *Int. J. Numer. Methods Fluids*, **23**, 445–454 (1996).
31. W.E. Cummins, *The forces and moments acting on a body moving in an arbitrary potential stream*, David Taylor Model Basin, Rep. No. 708, 1953.
32. L. Landweber and C.S. Yih, 'Forces, moments, and added masses for Rankine bodies', *J. Fluid Mech.*, **1**, 319–336 (1956).
33. M.A. Jaswon and G.T. Symm, *Integral Equation Methods in Potential Theory and Elastostatics*, Section 10.5, Academic Press, New York, 1977.
34. R. Piessens and M. Branders, 'Numerical solution of integral equations of mathematical physics, using Chebyshev polynomials', *J. Comput. Phys.*, **21**, 178–196 (1976).
35. K.E. Atkinson, 'A survey of boundary integral equation methods for the numerical solution of Laplace's equation in three dimensions', in M.A. Golberg (ed.), *Numerical Solution of Integral Equations*, Plenum Press, New York, 1990.
36. S.A. Yang and A.T. Chwang, 'An experimental study of nonlinear waves produced by an accelerating plate', *Phys. Fluids*, **4**, 2456–2465 (1992).